

UNSTEADY PDE-CONSTRAINED OPTIMIZATION WITH SPECTRAL ELEMENTS USING PETSC AND TAO*

OANA MARIN[†], EMIL CONSTANTINESCU[‡], AND BARRY SMITH[§]

Abstract. Solving optimization problems where the objective function depends on the solution to partial differential equations (PDEs) entails combining expertise from multiple areas, including simulation, computation of derivatives, and optimization algorithms. The Portable, Extensible Toolkit for Scientific computation (PETSc) together with its companion package, the Toolkit for Advanced Optimization (TAO), is an integrated numerical software library that contains an algorithmic/software stack for solving linear systems, nonlinear systems, ordinary differential equations, differential algebraic equations, and large scale optimization problems. It is an ideal tool for performing PDE-constrained optimization. This paper explains the algorithm and software stack used by PETSc/TAO and demonstrates its use for linear and nonlinear time-dependent problems using the spectral method in space, both one and two dimensional, high-order methods in time, and gradient-based methods for the PDE-constrained optimization.

Key words. adjoint, PETSc, PDE-constrained optimization, TAO, spectral element method

AMS subject classifications. 68Q25, 68R10, 68U05

1. Introduction. Fitting, either numerical or experimental, observations to determine parameters, identifying boundary conditions that satisfy certain observations, optimizing an objective (also called *cost*) function of the solution, accelerating simulations through their long transients (the spin-up problem [13]), and many more operations fall within the field of partial differential equation (PDE)-constrained optimization and inverse problems. Despite their widespread utility, the solution of of such problems are plagued by bottlenecks, including mathematical issues of ill-posedness, sensitivity to errors, high computational costs, high input-output costs, and software complexity. Several codes, such as JuMP [5], and Python libraries address these issues; however, many exhibit limitations for large-scale problems. To provide a framework for robustly tackling such problems we leverage the extensive range of methods available in both the Portable, Extensible Toolkit for Scientific computation (PETSc) [2] and the Toolkit for Advanced Optimization (TAO) [19],

Time-dependent PDE-constrained optimization problems can be posed in two ways: either by fully discretizing, in both space and time, the entire Karush-Kuhn-Tucker (KKT) system (that is, solving for all unknowns at all time steps simultaneously, sometimes called the *all-at-once* approach) [11] or by decoupling the direct problem and its adjoint [8], [21], [10], [23], [7] and solving the optimization problem via a forward/backward time-stepping loop, with appropriate initial and boundary conditions depending on the objective function. This work focuses on the latter, in particular on discrete adjoint approaches, outlining aspects of error analysis and efficient implementation approaches.

The core strategy presented in this study is to solve the inverse (or PDE-constrained optimization) problem in a purely nonlinear manner. Considerable work has previously relied on *linearized adjoints*; that is, the model is first linearized, and the adjoints are computed for that linearized problem [22]. Here we showcase the solution of the nonlinear

*Submitted to the editors DATE.

[†]Mathematics and Computer Science Division, Argonne National Laboratory, Argonne, IL (oanam@mcs.anl.gov).

[‡]Mathematics and Computer Science Division, Argonne National Laboratory, Argonne, IL (emconsta@anl.gov).

[§]Mathematics and Computer Science Division, Argonne National Laboratory, Argonne, IL (bsmith@mcs.anl.gov).

time-dependent viscous Burgers equation utilizing PETSc with TAO, both in one and two dimensions.

In our previous work [24], we addressed the data and computational intensity aspects of PDE-constrained optimization, aspects that are often overlooked. The data intensity for nonlinear problems stems from the nature of the backward-in-time component, which depends at every time instance on its forward counterpart. A robust treatment for balancing the compute time versus trajectory storage has been implemented in PETSc, using essentially the same techniques (utilizing the checkpointing algorithm *revolve* [9]) as in [24], for time-stepping routines for ordinary differential equations (ODEs) [26] and differential algebraic equations (DAEs). Here we extend that treatment to PDEs.

A property well known to the PDE optimization community is that continuous derivatives of the adjoint equation differ in nature from their discrete counterpart and may provide different gradients that affect the convergence of the optimization algorithm. We do not consider this issue in this paper, focusing only on discrete adjoint approaches. We note, however, that the SUNDIALS package [12] provides continuous adjoint capabilities [25]. Spectral element methods provide the spatial discretization with the highest accuracy per grid point of all currently available numerical schemes. Although the accuracy in the numerical solution does not imply directly faster convergence for the optimization step, it is valuable in approximating the gradient better. A novel long-term goal of our work is to equip the solvers with a combined space/time error analysis to facilitate studies of the impact of these errors on the optimization step. The relevance of this addition cannot be stressed enough, since the errors in the gradient computation tend to slow the convergence rate of the optimization algorithm and since errors in the forward simulation result in errors in the computed optimal solution or even convergence to the wrong solution.

The paper is organized as follows. The time-dependent PDE-constrained optimization problem is stated in an operator fashion, that allows for any operator such as diffusion, advection, or nonlinear ones such as the $u \cdot \nabla u$ operator in Burgers equation. The differences between the one and two dimensions are tracked at every step. Then the main aspects of a spectral element method are presented together with a brief discussion of its error analysis. This is followed by a discussion of the discrete adjoint approach. We then present an overview of PETSc ODE/DAE integrators and their adjoint solvers, followed by a description of TAO and its gradient-based solvers. The results section focuses on the complete solution process for performing PDE-constrained optimization using the spectral element method and PETSc/TAO, focusing mainly on nonlinear problems. The final section briefly summarizes our conclusions and future work.

2. Problem formulation. The aim of this work is to establish software for the systematic solution of PDE-constrained optimization problems. We denote a generic unsteady PDE model by

$$(1) \quad \begin{aligned} u_t &= P[u], \quad x \in \Omega \\ B[u|_{\partial\Omega}](t) &= u_b(t), \\ u(x, 0) &= u_0(x), \end{aligned}$$

where $P[u]$ is a stand-in operator for derivatives controlling the spatial behavior of the solution u (this is not the most general notation since for some PDEs there may be also a dependence on the spatial coordinates). The boundary condition u_b is provided with an operator $B[u]$, which is the identity for Dirichlet boundary conditions or a derivative for Neumann boundary conditions. This notation does not exclude periodic boundary

conditions. For simplicity, in most of the presentation we assume only homogeneous Dirichlet and/or periodic boundary conditions; that is, $u|_{\partial\Omega}(t) = 0$. However, this is not a limitation in PETSc.

Unless otherwise indicated, we assume that all functions in this manuscript are in K , a subset of $L^2(\Omega) = \{u : \Omega \rightarrow \mathbb{R} \mid (\int_{\Omega} |u|^2 d\Omega)^{1/2} < \infty\}$. Also we assume that the subset K is chosen such that the boundary conditions of the differential equations are satisfied. It is possible to express boundary conditions of the PDE as additional constraints; however, in the current framework we presume they are embedded in the discretization.

The optimization problem we seek to solve is

$$(2) \quad \min_{u_0, u \in K} \mathcal{J}(u), \quad s.t. \\ u_t = P[u], \quad \text{with } u|_{t=0} = u_0 \text{ and } B[u|_{\partial\Omega}](t) = u_b(t).$$

The objective functional is defined as

$$(3) \quad \mathcal{J}(u) = \int_0^T \int_{\Omega} g[u] \delta(x - x_s, t - t_r) dt d\Omega,$$

where the Dirac delta indicates whether we may have only discrete points x_s and t_r . A common occurrence in the field of inverse problems is to have only a limited set of observations in space, at sensor locations x_s , in which case the objective functional defined above continuously would take only a sparse set of values. In this case we restrict ourselves to spatially continuous data and consider the set of observation points t_r to be denoted by $R = \{t_r \in \mathbb{R}\}$. If the objective functional is available only at time horizon T , then we can write

$$\mathcal{J}(u) = \int_0^T \int_{\Omega} g[u] \delta(\cdot, t - T) dt d\Omega = \int_{\Omega} g[u(T)] d\Omega.$$

For simplicity we consider only PDE-constrained optimization problems where the control variables are the initial conditions u_0 . However, general controls are fully supported by PETSc.

An important special case is the data assimilation problem for which we seek the initial condition u_0 that leads at the *time horizon* T , to a solution $u(T)$ that matches a reference solution u_d . The standard objective functional that minimizes the difference between u and the reference solution u_d is

$$(4) \quad \mathcal{J}(u) = \int_{\Omega} (u(T) - u_d)^2 d\Omega.$$

3. Treatment of partial differential equations. We focus on discretizations stemming from methods based on variational (weak) formulations, such as finite elements, or spectral elements. For the weak form of a partial differential equation we seek u in K with the property that the residual is orthogonal to the set of all test functions, that is,

$$\int_{\Omega} (u_t - P[u]) v d\Omega = 0$$

for all v in K . Since nonlinear problems are the most challenging for constrained optimization we consider operators of the form $P[u] = \nu \Delta u - u \cdot \nabla u$, where ν represents the viscosity. We apply integration by parts to obtain the continuous Galerkin formulation

$$(5) \quad \int_{\Omega} u_t v d\Omega + \int_{\Omega} v(u \cdot \nabla u) d\Omega - \int_{\Omega} \nu \nabla u \nabla v d\Omega + \int_{\partial\Omega} v \frac{\partial u}{\partial n} d\partial\Omega = 0,$$

where n is the outward-facing normal. The boundary term vanishes since $u, v \in K$. The operator $P[u]$ incorporates all the classes of problems we treat here and can be reduced either to a pure diffusion problem by removing the gradient term or to a linear advection problem by replacing u with a constant velocity a .

For the two-dimensional cases we consider a similar operator $P[\mathbf{u}] = \nu\Delta\mathbf{u} - \mathbf{u} \cdot \nabla\mathbf{u}$, where the higher dimension is apparent in the boldface convention of the higher dimension vector \mathbf{u} . We note that in a two-dimensional setup the unknown $\mathbf{u} = [u, v]$ has two degrees of freedom, which translate into two coupled equations with the right-hand side

$$(6) \quad P \begin{bmatrix} u \\ v \end{bmatrix} = \begin{bmatrix} \nu\Delta u - u\nabla_x u - v\nabla_y u \\ \nu\Delta v - u\nabla_x v - v\nabla_y v \end{bmatrix}.$$

The weak formulation for the operator $P[\mathbf{u}]$ is identical to the one-dimensional formulation, and we do not reiterate it.

3.1. Temporal discretization in PETSc. The PETSc framework is aimed at universal solutions adaptable to any time integration strategy. It is therefore natural to consider a semi-discretization of the partial differential operators. Let us assume that the spatial discretization of the operators $P[u]$ is given as $\bar{P}[\bar{u}]$. Then the semi-discretization is

$$(7) \quad \frac{d\bar{u}}{dt} = \bar{P}[\bar{u}],$$

which is a form that can encapsulate both PDEs and ODEs. Although in the current work we treat only PDEs we will at times refer to the semi-discrete form as an ODE.

Equation 7 is integrated in time either explicitly by using a standard numerical integrator [2, 1] or implicitly as a nonlinear equation via Newton-type methods. Therefore it may be necessary to know the Jacobian

$$J[u] = \frac{dP[u]}{du},$$

which can be readily derived from the semi-discrete form, as will be outlined in Section 3.2. The Jacobian is required only for implicit/nonlinear solvers or for the discrete adjoint equation as will be seen in Section 4.2.1.

3.2. Spectral element method. Based on the weak form given by Equation 5, several discretizations are suitable, including the finite element method, spectral element method, or discontinuous Galerkin method. The spectral element method is a subclass of Galerkin methods, or weighted residual methods, that minimize the error of the numerical computation in the energy norm over a chosen space of polynomials or, equivalently, require the error to be orthogonal to the subspace defined by the spectral elements. These concepts are detailed in [4].

In the following we illustrate the spectral element discretization for Equation 5. The domain $\Omega = \cup_{e=1, M} \Omega_e$, is decomposed into M non-overlapping subdomains Ω_e , termed elements, over which the data will be represented by orthogonal polynomials.

The space of polynomials of order N defined over an element Ω_e , $e = 1, \dots, E$, is

$$\mathbb{P}_{N,E} = \{\phi | \phi \in L^2(\Omega); \quad \phi|_{\Omega_e} \text{ polynomial of degree } \leq N\}.$$

Subsequently $K_N = K \cap \mathbb{P}_{N,E}$. In the polynomial space K_N we represent the numerical solution as $u(x) = \sum_{i=0}^N u_i \phi_i(x)$.

The discrete point distribution x can be either a Chebyshev grid or a Legendre grid, consistent with the polynomial discretization. The current work is performed by using Legendre polynomials and Gauss-Legendre-Lobatto (GLL) grids, since this representation imposes less rigid stability restrictions on the time-steppers, having a smaller clustering of gridpoints at the boundary ends.

In either case the polynomials are orthogonal $\int_{\Omega} \phi_i \phi_j d\Omega = \delta_{ij}$. To proceed with the numerical discretization, we plug the ansatz into Equation 5 to obtain

$$(8) \quad \frac{\partial}{\partial t} \sum_{i,j=0}^N u_i v_j \underbrace{\int_{\Omega} \phi_i(x) \phi_j(x) d\Omega}_{M_{ij}} - \nu \sum_{i,j=1}^N u_i v_j \underbrace{\int_{\Omega} \phi'_i(x) \phi'_j(x) d\Omega}_{K_{ij}} + \sum_{i,j,k=1}^N u_k u_i v_j \underbrace{\int_{\Omega} \phi_k(x) \phi'_i(x) \phi_j(x) d\Omega}_{D_{ij}} = 0,$$

where M_{ij} is the mass matrix, K_{ij} is the stiffness matrix, and D_{ij} is the differential matrix. Note that in this case the contribution of the basis ϕ_k is present only as integration weights since the polynomials ϕ_k evaluate to unity on the Ω grid. Because of the orthogonality properties of the polynomials, the mass matrix is diagonal.

We can write the equations in algebraic form and scale out the test function v to obtain

$$(9) \quad M \frac{d\bar{u}}{dt} = \nu K \bar{u} - \bar{u} \circ D \bar{u},$$

where $\bar{u} = (u_0, u_1, \dots, u_N)$. Here we introduce the notation \circ to designate the Hadamard product, also known as pointwise multiplication.

If we assume $\Omega_e = [a, b]$ and define the reference element $\hat{\Omega} = [-1, 1]$, then for $x \in \Omega_e$ and $r \in \hat{\Omega}$ the mapping from each element to the reference element is

$$x = a + \frac{b-a}{r+1}.$$

This mapping introduces a scaling factor for each element, given by the Jacobian of the coordinate transformation. Note that for curvilinear geometries as well as for variable coefficients ν the operators K and D will have more complex expressions that take into account the Jacobian and multiply the variable coefficients.

For an implicit solver, as well as nonlinear Newton solvers, Equation 9 requires the Jacobian of the right-hand side. We note the Jacobian is required in its transposed form by the discrete adjoint solver. For the right-hand side $\bar{P}\bar{u} = \nu K \bar{u} - \bar{u} \circ D \bar{u}$ the Jacobian becomes

$$(10) \quad \frac{d\bar{P}}{d\bar{u}} = \nu K - (\text{diag}(D\bar{u}) + \text{diag}(\bar{u}) \circ D),$$

where we use the definition of the derivative of a Hadamard product to compute the derivative of the nonlinear term.

Two-Dimensional case. Consider the domain $\Omega = [-1, 1]^2$ discretized in N GLL points. The two-dimensional basis function is separable $\phi_k(x, y) = \phi_i(x) \phi_j(y)$ where $i, j = 1, \dots, N$ and $k = i + (N+1) \cdot j$. The ansatz on the solution is similar to the one-dimensional-case

$$u(x, y) = \sum_{i=0}^M \sum_{j=0}^N u_{ij} \phi_i(x) \phi_j(y).$$

We note that optimization algorithms, especially for time-dependent problems, are computationally expensive. For example for an optimization that requires m iterations, one needs to perform $2m$ solves each of N time steps, where the backward solution is in practice more expensive than the forward. It is crucial to employ any computational acceleration possible, even one providing negligible speedup, since any speedup accumulates significantly with the number of iterations.

The separability of the basis functions allows us to represent the operators \mathbf{K} , \mathbf{D} , \mathbf{M} as tensor products in each dimension. For example, the stiffness operator $\mathbf{K} = M \otimes K + K \otimes M$, where we presume the same discretization in both x and y directions, and the operator K is the same as in one dimension. The advantage of this representation is that operators can now be applied in a more efficient matrix-free form, namely $\mathbf{K} \bar{\mathbf{u}} = (M \otimes K + K \otimes M)\bar{\mathbf{u}}$. By virtue of the tensor product we can evaluate each matrix-vector multiplication without unrolling the unknown variable \mathbf{u} but by replacing it with two matrix-matrix products, $(M \otimes K)\bar{\mathbf{u}} = K^T \bar{\mathbf{u}} M$.

Let us consider the operators

$$\begin{aligned}\mathbf{M} &= (M \otimes M) \\ \mathbf{K} &= (M \otimes K + K \otimes M).\end{aligned}$$

The partial differential equation is similar to the one dimensional counterpart. However, we will expand the the nonlinear terms for further clarifying the structure of the Jacobian.

$$(11) \quad \begin{aligned}\mathbf{M} \frac{d\bar{\mathbf{u}}}{dt} &= \nu \mathbf{K} \bar{\mathbf{u}} - \underbrace{\bar{u} \circ (D \otimes M) \bar{u} + \bar{v} \circ (M \otimes D) \bar{u}}_{\mathcal{N}(\bar{u})} \\ \mathbf{M} \frac{d\bar{\mathbf{v}}}{dt} &= \nu \mathbf{K} \bar{\mathbf{v}} - \underbrace{\bar{u} \circ (D \otimes M) \bar{v} + \bar{v} \circ (M \otimes D) \bar{v}}_{\mathcal{N}(\bar{v})}\end{aligned}$$

The Jacobian of the right-hand side of Burgers equation is linear for the first two terms. However it has a more complicated expression for the nonlinear parts.

$$(12) \quad J = \begin{bmatrix} \mathbf{K} & 0 \\ 0 & \mathbf{K} \end{bmatrix} + \begin{bmatrix} \frac{d\mathcal{N}(\bar{u})}{d\bar{u}} & \frac{d\mathcal{N}(\bar{u})}{d\bar{v}} \\ \frac{d\mathcal{N}(\bar{v})}{d\bar{u}} & \frac{d\mathcal{N}(\bar{v})}{d\bar{v}} \end{bmatrix}$$

For efficiency we implement the Jacobian in a matrix-free fashion as applied to a vector $\mathbf{w} = (w_u, w_v)$. An explicit expression of the Jacobian components is

$$\begin{aligned}Jw_u &= w_u \circ (D \otimes M) \bar{u} + \bar{u} \circ ((D \otimes M)w_u) + \bar{v} \circ ((M \otimes D)w_u) + w_v \circ ((M \otimes D) \bar{u}) \\ &\quad + (M \otimes K + K \otimes M)w_u, \\ Jw_v &= w_u \circ (D \otimes M) \bar{v} + \bar{u} \circ ((D \otimes M)w_v) + \bar{v} \circ ((M \otimes D)w_v) + w_v \circ ((M \otimes D) \bar{v}) \\ &\quad + (M \otimes K + K \otimes M)w_v.\end{aligned}$$

This approach to computing the Jacobian vector product is only two tensor products more expensive than the right-hand side of the PDE, given by Equation 11.

3.3. PETSc implementation. The PETSc time-stepping component TS provides access to a large number of ODE integrators including explicit, implicit, and implicit-explicit (IMEX) methods. IMEX integrates the stiff portion of the equation implicitly and the other portion explicitly; however, in the present work we use only implicit and explicit time integrators.

The linear and nonlinear systems that arise in the implicit solvers may be solved by using any of PETSc's algebraic solvers, as well as solvers from other packages such as hypre [6] or SuperLU_Dist [15]. The TS integrators are generally multistage integrators, with local and global error estimate adaptive controllers, although PETSc does provide some multistep integrators. Details on solvers and integrators in PETSc may be found in [2].

The PETSc interface for solving time-dependent problems is organized in a general fashion around the following form of an implicit differential equation:

$$F(t, u, \dot{u}) = G(t, u), \quad u(t_0) = u_0.$$

If the matrix $F_{\dot{u}}(t) = \partial F / \partial \dot{u}$ is nonsingular, then this is an ordinary differential equation and can be transformed to the standard explicit form. For a PDE/ODE we write $F(t, u, \dot{u}) = M\dot{u}$ and $G(t, u) = \bar{P}[\bar{u}]$, or $F(t, u, \dot{u}) = \dot{u}$ and $G(t, u) = M^{-1}\bar{P}[\bar{u}]$, since the representation of any semi-discrete partial differential equation is in essence an ODE. For ODEs with nontrivial mass matrices, such as those arising in the finite/spectral element method, the implicit/DAE interface can significantly reduce the overhead in preparing the system for algebraic solvers by having the user assemble the correctly shifted matrix. The user provides function pointers and pointers to user-defined data for each operation, such as the function $F()$ needed by the library. This approach allows full utilization from C, Fortran, Python, and C++ since all these languages support these constructs, whereas, for example, the use of classes would limit the language portability.

For explicit methods one needs only to specify $\bar{P}[\bar{u}]$ in the function `TSSetRHSFunction`, while for implicit methods the user provides also the function $\frac{d\bar{P}}{d\bar{u}}$ in `TSSetRHSJacobian` [1]. Following is an example listing for specifying a linear ODE that is to be solved with the explicit Runge-Kutta integrators.

```

TSCreate(MPI_Comm comm, TS *ts);
TSSetType(TS ts, TSType type);
TSSetProblemType(TS ts, TS_LINEAR);
TSSetType(TS ts, TSRK);
5 TSSetTime(TS ts, 0.0);
TSSetTimeStep(TS ts, PetscReal initial_dt);
TSSetMaxTime(TS ts, PetscReal Tend);
TSSetRHSFunction(TS ts, Vec r, (*f)(TS, PetscReal, Vec, Vec, void*),
void *ctx);
TSSetRHSJacobian(TS ts, Mat mat, Mat pmat, (*j)(TS, PetscReal, Vec,
Mat, Mat, void*), void *ctx);
10 TSSolve(TS ts, Vec u);

```

4. PDE-constrained optimization. Several approaches are available when dealing with PDE-constrained optimization problems; however, we prefer the Lagrange-multiplier framework, which is used in both continuous and discrete adjoints. The derivation of each adjoint formulation is specific to the problem at hand; both discrete and continuous adjoints can be traced back to a Lagrangian multiplier formulation where the adjoint is obtained from the forward problem under the appropriate inner product.

4.1. Using adjoints for optimization. Equation 2 is posed as an optimization of a functional subject to a time-dependent PDE-constraint. Given that the Lagrangian multiplier relies on inner products for determining the minimum/maximum of a functional, we need to define the inner product for PDE constraints in a Hilbert space as

$$(13) \quad (u, v) = \int_0^T \int_{\Omega} u \cdot v \, d\Omega dt.$$

Equation 2 can now be framed in the Lagrangian multiplier framework, with v playing the role of Lagrange multiplier or adjoint variable

$$(14a) \quad \min_{u_0, u \in K} \max_{v \in K} \mathcal{L}(u, v), \text{ where}$$

$$(14b) \quad \mathcal{L}(u, v) = \min_{u_0, u \in K} \max_{v \in K} \mathcal{J}(u) + \int_0^T \int_{\Omega} (v(u_t - P[u])) d\Omega dt.$$

The Lagrangian has a stationary point for each extremum of the original problem (plus possibly additional stationary points), and the objective functional is defined as in Equation 3. Here, however, we operate mainly with an objective function as provided by Equation 4.

The continuous adjoint derivation leads to a closed form PDE for the adjoint variable v , while the discrete adjoint requires evaluations at every time-step. For a semi-discrete partial differential equation $\bar{u}_t = \bar{P}[\bar{u}]$ let us consider a general model of a time-stepper:

$$(15) \quad \bar{u}_{i+1} = A(\bar{u}_i, \bar{P}[\bar{u}_i]).$$

This particular model is valid for explicit time-steppers. For implicit ones we need to consider the right-hand side as an operator applied to \bar{u}_{i+1} instead; however, the treatment is similar.

Given that we are in a discrete framework, the inner product defined in Equation 13 has to be discretized. Considering that the inner product in space is $(u, v) = u^T M v$, where M is the mass matrix, and for the time integration we take the Riemann sum, we can express the total inner product in Problem 14a as

$$\int_0^T \int_{\Omega} (v(u_t - P[u])) d\Omega dt \approx \sum_{i=1}^N v_i^T M (\bar{u}_i - A(\bar{u}_{i-1}, \bar{P}[\bar{u}_{i-1}])),$$

where we use the convention that $u_0 = u(0)$ and $u_N = u(T)$. After a shift and rewrite of the summation bounds; the total Lagrangian multiplier can be represented as

$$(16) \quad \mathcal{L}(\bar{u}, v) = \bar{\mathcal{J}}(\bar{u}) + \sum_{i=0}^{N-1} v_i^T M \bar{u}_i - v_{i+1}^T M A(\bar{u}_i, \bar{P}[\bar{u}_i]) + v_N^T M \bar{u}_N.$$

To identify the adjoint, we now require that all derivatives of \mathcal{L} cancel, i.e.

$$(17) \quad \frac{\partial \mathcal{L}}{\partial \bar{u}_i} = \frac{\partial \bar{\mathcal{J}}}{\partial \bar{u}_i} - v_i^T M + \left(\frac{\partial A(\bar{u}_i, \bar{P}[\bar{u}_i])}{\partial \bar{u}_i} \right)^T v_{i+1}^T M = 0$$

$$(18) \quad \frac{\partial \mathcal{L}}{\partial \bar{u}_N} = \frac{\partial \bar{\mathcal{J}}}{\partial \bar{u}_N} - v_N^T M = 0$$

$$(19) \quad \frac{\partial \mathcal{L}}{\partial \bar{u}_0} = \frac{\partial \bar{\mathcal{J}}}{\partial \bar{u}_0} + \left(\frac{\partial A(\bar{u}_0, \bar{P}[\bar{u}_0])}{\partial \bar{u}_0} \right)^T v_1^T M = 0$$

The adjoint equation to be solved is provided by Equation 17, while Equation 18 gives the initial condition for the return, and Equation 19 is in fact the gradient to be used in the optimization step.

We now can analyze what the operator $\frac{\partial A(\bar{u}, \bar{P}[\bar{u}])}{\partial \bar{u}}$ translates into. To take the derivative of the operator A , we need to treat it via the implicit function theorem where \bar{u} and $\bar{P}[\bar{u}]$ are treated as independent variables yielding

$$(20) \quad \left(\frac{\partial A(\bar{u}, \bar{P}[\bar{u}])}{\partial \bar{u}} \right)^T = \left(\frac{\partial A(\bar{u}, \bar{P}[\bar{u}])}{\partial \bar{u}} + \frac{\partial A(\bar{u}, \bar{P}[\bar{u}])}{\partial \bar{P}[\bar{u}]} \frac{\partial \bar{P}[\bar{u}]}{\partial \bar{u}} \right)^T,$$



Figure 1: Work-flow for optimization problems using adjoints. Note that we already included the time reversal (the instances v_i are in fact v_{N-i})

where, for example, for a spatial operators such as $P = K\bar{u} + u \circ D\bar{u}$ the Jacobian is given by Equation 10. Note that the adjoint formulation relies on the Jacobian transpose. Typically the Jacobian is readily available for implicit time integrators.

The Jacobian of the operator A depends on which time integration scheme is used, and it leads to the tableau of the time integrator. We briefly illustrate how this behaves for forward Euler. The model $\bar{u}_{i+1} = A(\bar{u}_i, \bar{P}[\bar{u}_i])$ becomes

$$\bar{u}_{i+1} = u_i + \Delta t \bar{P}[\bar{u}_i]$$

and the derivative of A is now calculated by using Equation 20 and becomes

$$(21) \quad \frac{\partial A(\bar{u}, \bar{P}[\bar{u}])}{\partial \bar{u}} = I + \Delta t \frac{\partial \bar{P}[\bar{u}]}{\partial \bar{u}}.$$

By setting $\nabla_{u_i} \mathcal{L} = 0$ in Equation 17 we obtain the adjoint equation based on the forward Euler with the typical time reversal $i = N, \dots, 1$:

$$(22) \quad v_i = v_{i+1} + \Delta t \frac{\partial \bar{P}[\bar{u}]}{\partial \bar{u}}^T v_{i+1}.$$

Regarding the objective functional, we distinguish between the two cases: time dependent or not. The continuous Dirac delta $\delta(t - t_r)$ becomes for a set $\bar{R} = \{r \in \mathbb{N}\}$ the discrete Kronecker delta δ_{kr} , and the derivative of the Jacobian is

$$\begin{aligned} \frac{\partial \mathcal{J}}{\partial \bar{u}_i} &= \frac{\partial}{\partial \bar{u}_i} \sum_{k=1}^N M g[u_k] \delta_{kr} \\ &= \sum_{k=1}^N M \frac{\partial g[u_k]}{\partial \bar{u}_i} \delta_{kr} \\ &= \sum_{k=1}^N M \frac{\partial g[A^k(\bar{u}_{N-k}, \bar{P}(\bar{u}_{N-k}))]}{\partial \bar{u}_i} \delta_{kr} \\ &= M \frac{\partial g[(\bar{u}_N)]}{\partial \bar{u}_N} \sum_{k=i+1}^N \left(\prod_{j=k}^N \frac{\partial g[A(\bar{u}_{N-j}, \bar{P}(\bar{u}_{N-j}))]}{\partial \bar{u}_{N-j}} \right) \delta_{kr}. \end{aligned}$$

In this form, for R containing only the time instance T , we have the term δ_{kN} , which cancels all but the last product.

In this context we discretize in space using an identical integration scheme for the forward and backward problem and the same timesteps as used for the forward integration

to obtain the fully discrete adjoint formulation; however, time interpolation could be envisioned. The final gradient used by the TAO optimizer is provided by setting Equation 19 to zero.

Of course this procedure requires that the forward solution be available during the backward solve, which could be available either by writing/reading from file, or by storing in memory. This data management procedure is referred to as checkpointing and is available directly via the PETSc adjoint implementation, as will be described in Section ?? . We summarize the adjoint-based approach in Figure 1, where initial conditions for forward and adjoint solve are provided by the solution of Equation 18.

4.2. PETSc/TAO implementation. The PETSc interfaces for computing discrete adjoints are built on top of the ODE/DAE interface. We illustrate the adjoint derivation only for initial conditions; however, the framework allows also for optimization with respect to parameters p , such as the extended objective function

$$\mathcal{J}(u, p) = \int_0^T \int_{\Omega} g(u, p) \delta(x - x_p, t - t_r) dt d\Omega.$$

The adjoint integrator routines of PETSc provide the resulting gradients, using the adjoint v_0 for the objective with respect to initial conditions as provided by Equation 19 and the adjoint μ for the parameters computed as

$$(23) \quad \frac{\partial \mathcal{J}}{\partial p} = \mu + v_0 \left(\frac{\partial u_0}{\partial p} \right).$$

To compute the gradients the user first sets up the TS object for a regular forward run but with one additional function call, `TSSetSaveTrajectory(TS ts)`, and then calls `TSSolve()` in the usual manner.

The user must provide two vectors v_0 and μ (if there are no parameters beside the initial conditions, as is true in this paper, one can use `NULL` for the μ array). The v_0 vector has the same dimension and parallel layout as the solution vector for the ODE. However, this is not required by TAO. The μ vector has the same dimension as p ; when this size is small, usually all its elements are stored on the first MPI process, while the vector has no entries on the other processes. The vectors v_0 and μ both must be initialized by the user with the values provided by Equation 18 and $d\mathcal{J}/du$ and $d\mathcal{J}/dp$, respectively. Then the user calls

```
TSSetCostGradients(TS ts, 1, Vec *v0, Vec *mu);
```

If $F()$ is a function of p , the user needs also to provide its Jacobian with respect to p using the following

```
TSAdjointSetRHSJacobian(TS ts, Mat Amat, (*fp)(TS, PetscReal, Vec, Mat, void*), void *ctx)
```

The user then starts the backward run by calling the following.

```
TSAdjointSolve(TS ts);
```

For explicit methods where the user does not need to provide the Jacobian for the forward solve, one still does need to provide it for the backward solve and thus must call the following.

```
TSSetRHSJacobian(TS ts, Mat Amat, Mat Pmat, (*f)(TS, PetscReal, Vec, Mat, Mat, void*), void *fP);
```

If the objective function evaluation is needed, the value can be retrieved by calling the following.

```
TSGetCostIntegral(TS ts, Vec *q).
```

The discrete adjoint algorithm requires the forward states (and stage values in the context of multistage time-stepping methods) in order to evaluate the Jacobian matrices during the adjoint (backward) run. The trajectory information is managed by an extensible abstract trajectory object, `TSTrajectory`, that has multiple implementations. This object provides support for storing checkpoints at selective time steps and recomputing the missing information. The `revolve` [9] library is used by `TSTrajectory` to generate an optimal checkpointing schedule that minimizes the recomputations given a limited number of available checkpoints; see Section ??.

PETSc and the `revolve` library also provide an optimal multistage checkpointing scheme that uses both RAM and disk for storage.

4.2.1. TAO: gradient-based optimization. The Toolkit for Advanced Optimization is a scalable software library for solving large-scale optimization applications on high-performance architectures. It is motivated by the scattered support for scalable parallel computations and the lack of reuse of linear algebra software in currently available optimization software.

TAO contains unconstrained minimization, bound-constrained minimization, nonlinear complementary, nonlinear least-squares solvers, and solvers for optimization problems with PDE-constraints. The structure of these problems can differ significantly, but TAO has a similar interface to all its solvers.

TAO applications follow an ordered set of procedures for solving an optimization problem in a way similar to the ODE/DAE integrators.

```
TaoCreate(MPI_Comm comm, Tao *tao);
TaoSetType(Tao tao, TaoType type);
TaoSetInitialVector(Tao tao, Vec x);
TaoSetObjectiveAndGradientRoutine(Tao tao, (*fg)(Tao, Vec,
    PetscReal*, Vec, void*), void *user);
5 /* The Hessian routine is optional */
TaoSetHessianRoutine(Tao tao, Mat H, Mat Hpre, (*fh)(Tao, Vec, Mat, Mat,
    void*), void *user);
TaoSetFromOptions(Tao tao);
TaoSolve(Tao tao);
```

Note that the solver algorithm is selected through the function `TaoSetType()` and, like virtually all PETSc and TAO options, can be overridden at runtime by using an options database with an appropriate call to `TaoSetFromOptions()`. Through this database, the user not only can select a minimization method but also can prescribe the convergence tolerance, set various monitoring routines, set iterative methods and preconditions for solving the linear systems, and so forth.

For gradient-based optimizers, as used in this paper, both the objective function and the gradient function must be provided by the user. Often they can most efficiently be provided as a single function with the following.

```
TaoSetObjectiveAndGradientRoutine(Tao, (*fg)(Tao, Vec, PetscReal*,
    Vec, void*), void *);
```

TAO provides two gradient-based optimizers appropriate for the optimizations considered in this paper. The *limited-memory, variable-metric* (LMVM) [16] method computes a

positive-definite approximation to the Hessian matrix from a limited number of previous iterates and gradient evaluations. A direction is obtained by solving the system of equations

$$H_k d_k = -\nabla f(x_k),$$

where H_k is the Hessian approximation obtained by using the Broyden update [20] formula. The inverse of H_k can readily be applied to obtain the direction d_k . Having obtained the direction, a Moré-Thuente line search [18] is applied to compute a step length, τ_k , that approximately solves the one-dimensional optimization problem

$$\min_{\tau} f(x_k + \tau d_k).$$

The current iterate and Hessian approximation are updated, and the process is repeated until the method converges. This algorithm is the default unconstrained minimization solver in TAO. All the numerical studies in this paper utilize LMVM.

4.3. PETSc implementation of PDE-constrained optimization. We utilize both the ODE/DAE integrators of TS and the gradient-based optimization of TAO for PDE-constrained optimization. For spatial discretization the user (or an appropriate library) needs to provide the function evaluations and the associated Jacobians that arise from the space-dependent operators equipped with the appropriate boundary conditions. In addition, the user must provide the objective function; essentially everything else is handled by the libraries. We present the PETSc TS code in Listing 1 that computes the objective function and its gradient (via adjoints, see Equation 17) for our model problem.

Listing 1: PDE-constrained optimization: Computing gradients via adjoints

```

/* f will contain the objective function value and G the gradient
*/
FormFunctionAndGradient(Tao tao,Vec initialconditions,PetscReal *
    f,Vec G,AppCtx *appctx)

VecCopy(initialconditions,appctx->current_solution)
5 TSSolve(appctx->ts,appctx->current_solution)

VecWXPY(G,-1.0,appctx->current_solution,appctx->reference)

10 /* Compute the objective function */
VecDuplicate(G,&temp)
VecPointwiseMult(temp,G,G)
VecDot(temp,appctx->mass,f)
VecDestroy(&temp)

15 /* Compute initial conditions for the adjoint integration. */
VecScale(G,-2.0)
VecPointwiseMult(G,G,appctx->mass)
TSSetCostGradients(appctx->ts,1,&G,NULL)

20 TSAdjointSolve(appctx->ts)

```

5. Computational challenges. Setting aside the inherent mathematical hurdles of PDE-constrained optimization problems, such as ill-posedness and achieving convergence

Several computational bottlenecks also exist. The total computational time of an optimization loop is $2Nm$, where N is the number of time steps per solve from t_0 to time horizon T , and m is the total number of iterations of the optimization algorithm. The number of iterations depends on the quality of the gradient; thus, accuracy in the computation has a direct impact. Moreover the time per time step is $2m$ times more expensive than for a regular simulation and any speedup accrued at the time-step level leads to a dramatic decrease in total time. As illustrated in Figure 1, at every time-step of the adjoint solve the corresponding forward solution is needed. This raises the question of whether it is more efficient to store the solution of the forward to file or in memory or to recompute the solution. Of course ideally one would seek to find the break-even point between retrieving and recomputing the solution, which will be discussed in Section ??.

5.1. Impact of accuracy. To assess the error incurred in the spatial spectral element discretization, we use the a posteriori spectral error analysis suggested in [17]. An exhaustive review can be found in [14]. Considering the discrete solution $u_N \in X_N$ (the Hilbert space of polynomials of order N), an extrapolated solution $\tilde{u} \in X_M$ where X_m is a space of polynomials of order $M \gg N$, and the exact solution u , we can bound the error by

$$\|u - u_N\| \leq \underbrace{\|u - \tilde{u}\|}_{\text{extrapolation error}} + \underbrace{\|\tilde{u} - \Pi_N \tilde{u}\|}_{\text{truncation error}} + \underbrace{\|u_N - \Pi_N \tilde{u}\|}_{\text{quadrature error}},$$

where $\Pi_N u$ is the projection of u on a polynomial space of order N .

We identify the terms in the error as follows:

- *Extrapolation error* – error incurred by extrapolating the solution to a higher-order space (needed to identify the truncation error; this error is negligible)
- *Truncation error* – error incurred by the truncation to a lower-order space
- *Quadrature error* – error of the quadrature introduced by discretizing the weak formulation.

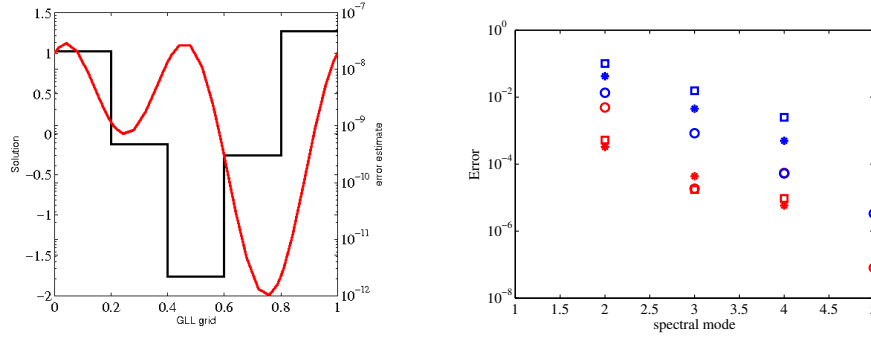
The final two errors are of similar size; and given that we are in a spectral element framework, the projection on an orthogonal polynomial space exhibits spectral decay. A simple derivation gives the leading-order term of the truncation in the error bound to ϵ_e with

$$\epsilon_e = \frac{a_N^2}{(2N + 2)/2},$$

where a_N can be approximated from a least-squares expansion as $a_N = ce^{-\sigma N}$, N is the number of degrees of freedom, σ is the slope of the decay, and c is a scaling factor.

The computational procedure is straightforward: Transform the velocity field, per element, into spectral space, where the decay can be viewed as a linear function in log scale, and compute both σ and c . For a given signal, such as that in Figure 2a, we obtain error bounds per element that are consistent with the fluctuations in the data.

The time integration error in PETSc can be tracked by using the built-in error estimation and error control mechanism (command line option `-g1ee`). This mechanism is implemented by changing the step size in order to maintain user-specified absolute, Tol_A , and relative, Tol_R , tolerances. The error estimate is based on the local truncation error, so for every step the algorithm verifies that the estimated local truncation error satisfies the tolerances provided by the user and computes a new step size. For multistage methods, the local truncation is obtained by comparing the solution u to a lower-order $\hat{p} = p - 1$ approximation, \hat{u} , where p is the order of the method and \hat{p} the order of \hat{u} .



(a) Solution to the heat equation (red) for a discretization of $N=8$ points over $E=5$ elements, and error bars (black) in log scale (right y axis) per element computed via the error estimator.

(b) Error computed per element. Sample elements 1:3 represented by different markers: spectral representation of the error in the signal (red), error estimate computed by the procedure (blue).

Figure 2: A posteriori error estimation for a spectral spatial discretization.

The adaptive controller at step n computes a tolerance level,

$$Tol_n(i) = Tol_A(i) + \max(|u_n(i)|, |\hat{u}_n(i)|)Tol_R(i),$$

and forms the acceptable error level, referred to as weighted local truncation error

$$wlte_n = \frac{1}{m} \sum_{i=1}^m \sqrt{\frac{\|u_n(i) - \hat{u}_n(i)\|}{Tol_n(i)}},$$

where the errors are computed componentwise and m is the dimension of u . If the infinity norm is used, then

$$wlte_n = \max_{1..m} \frac{\|u_n(i) - \hat{u}_n(i)\|}{Tol_n(i)}.$$

The error tolerances are satisfied when $wlte \leq 1.0$.

The next step size is based on this error estimate and determined by

$$(24) \quad \Delta t_{\text{new}}(t) = \Delta t_{\text{old}} \min(\alpha_{\text{max}}, \max(\alpha_{\text{min}}, \beta(1/wlte)^{\frac{1}{p+1}})),$$

where α_{min} and α_{max} keep the change in Δt to within a certain factor and $\beta < 1$ is chosen so that there is some margin to which the tolerances are satisfied and so that the probability of rejection is decreased.

The global error or a posteriori error (see [3] for a comprehensive discussion) represents the actual numerical error resulting after applying a time-stepping algorithm. Local error estimates cannot predict how those local errors will propagate through the simulation, and for some problems these local errors can grow to be larger than intended. We have begun to implement efficient global error estimators into the PETSc integrators beginning with the Runge-Kutta schemes. The estimators evolve the global error estimate along with the solution; in our strategy the internal calculations of the two quantities are overlapped by using a single scheme to evolve them simultaneously and efficiently [3].

The impact of the gradient quality on the overall optimization is illustrated in Figure 3.

5.2. Computational efficiency. Both the implementation and algorithm can have a high impact on the total time of the simulation. The best approach is to choose a scheme that has the lowest number of flops per accuracy threshold, and these methods are the ones with spectral accuracy. Of the spectral methods the spectral element has the great advantage that it is highly parallelizable and can be easily used to perform a matrix-free tensor product implementation per spectral element.

The computational complexity can be reduced from $\mathcal{O}(N^{2d})$ to $\mathcal{O}(N^{d+1})$, where d is the spatial dimension. Of course at first sight this brings no relevant gains in two dimensions; however, the highly vectorized structure of the tensor product multiplications allows efficient implementations (see [4] p.168).

6. Results. We present a set of problems: diffusion, advection-diffusion, and Burgers equation, in one dimension, and the viscous Burger's equation in two dimensions.

We note that diffusion-dominated problems, such as those studied here, are ill-conditioned since small perturbations in the initial conditions smooth away quickly. Thus, multiple initial conditions lead to the same final solution, which can be a challenge when solving inverse problems. Here we are not concerned with the issues of this ill-conditioning; rather we focus on explaining the process in detail and in understanding the error properties inherent in the discretizations and algorithms used.

All spatial operators are discretized by using the spectral element method, and the time integration is based on the TS capability of PETSc.

6.1. Convergence study. For convergence studies on the advection-diffusion equation we utilize the exact reference solution of the form

$$u(x, t) = \sum_{j=1}^{nc} a_j \sin(2\pi j(x - at)) e^{-\nu 4\pi^2 j^2 t},$$

where nc is 5 and the a_j are selected from a uniform distribution between 0.9 and 1. The initial guess is of the same form with t equal to zero and utilizing different random values. The diffusion coefficient ν is 0.00001, the advection speed a is 0.1, and the time horizon is 0.01. This choice of parameters renders the PDE convection dominated, which is particularly useful isolating the ill-posedness stemming from the diffusive component.

The tolerances for the TAO solver were set low so that they do not introduce any errors. The timestep was selected adaptively so that the error due to the time discretization is also small.

In Figure 3 we plot the convergence history for the iterations of optimization algorithm for a variety of h- and p-refinements. The L_2 norm of the error to the analytic optimization problem is plotted in Figure 4. As expected, the convergence is second order for h-refinement and spectral for p-refinement.

6.2. One-dimensional problems. Partial differential equations comprise three main classes of problems: elliptic, hyperbolic and parabolic. We focus here mainly on parabolic and hyperbolic types since these are commonly encountered in time-dependent contexts. We also consider a fully nonlinear case, the Burgers equation.

6.2.1. Diffusion. A diffusion problem with periodic boundary conditions and a viscosity parameter $\nu = 0.001$ is considered over the domain $[0, 1]$. The domain is discretized in five spectral elements each of polynomial order $N = 8$, and the time horizon of the forward problem is $T = 1$. We choose the reference function to be a solution to the heat equation. Specifically, $u_d = u(x, T_a)$, where we set $T_a = 3.0$. For the time horizon of the problem we choose $T = 1.0$. We seek again to optimize for the

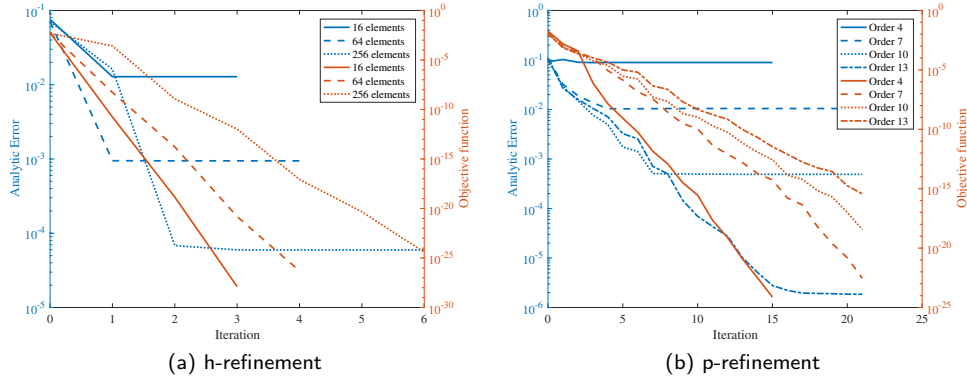


Figure 3: Convergence history of analytic solution and objective function.

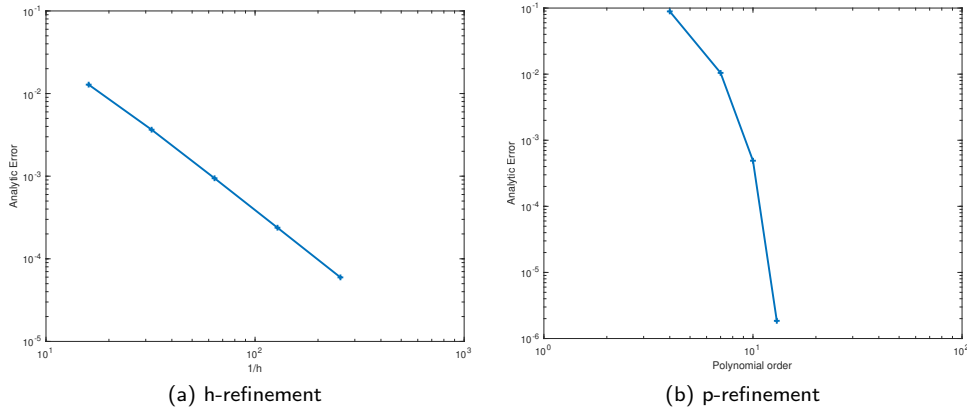


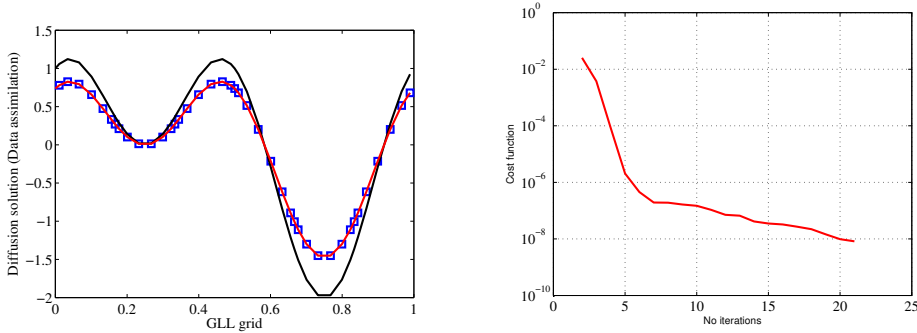
Figure 4: Analytic error with spatial refinement.

initial condition, by minimizing $J(u_0) = \int_{\Omega} (u(T) - u_d)^2 d\Omega$. The initial condition is $u_0 = u(x, 0) = (\sin(2\pi x) + \cos(4\pi x))$. Since the time horizon is $T = 1.0$ and the reference function is the solution at $T_a = 3.0$, we can compare the result of the optimization with the exact solution at $u(x, T_a - T)$ and identify the behavior of the errors.

The results are illustrated in Figure 5a and Figure 5b. We note a difference between the optimal and the reference solutions, which is natural given that the initial optimal condition has to decay for a time T to reach u_d .

Comparing the error of the optimal solution stemming from the optimization u_0^{opt} and the analytical solution at the same time instance $u(x, T_a - T)$, we note in Figure 5b that the error between the two is higher than the threshold imposed on the optimization. In this case the PDE error is a compound of the space $O(e^{-\sigma N})$ error and time errors, which for a third-order method are $O(\Delta t^3)$. We performed a spatial error analysis on this problem, described in Section 3.2, and in Figure 2a we illustrate for this particular case the spatial error on a per element basis. The upper bound of the spatial error is given at the leftmost element in this discretization and is of magnitude 10^{-7} . To observe this in

the full optimization setup, we chose a time step of size 10^{-5} , far lower than the stability requirements of the problem and impractical for computational purposes, but revealing for the spatial error, which we can see plateaus at 10^{-5} and is within the round-off vicinity of the spatial error. This is by no means an extensive study of errors but rather a prerequisite to a full-fledged analysis of the interplay between the convergence of the optimization and the error of the underlying PDE.



(a) Diffusion-constrained optimization: objective function (blue), optimal solution (red), initial condition at first iteration (black). (b) Diffusion-constrained optimization: objective function decay versus number of iterations.

Figure 5: Optimal initial conditions for the heat equation with a smooth reference function and time horizon $T=1$.

6.2.2. Advection-diffusion. The parameters used here are the advective velocity $a = 0.05$ and diffusion coefficient $\nu = 0.001$. The function we assess is a Gaussian advected to the left of the domain, and the solution is given as $u(x, t) = e^{-(x-5+at)^2} e^{-\nu t}$.

In Figure 7a we illustrate both the initial condition and desired solution we seek to attain at time horizon T . The objective function decay versus the number of iterations required for finding the initial condition u_0 is illustrated in Figure 6. For an admissible error in the solution of 10^{-8} we obtain the final optimal solution in Figure 7b. The optimization algorithm used here is the LMVM method, and the time stepper is an explicit Runge-Kutta of third-order accuracy. PETSc also provides adjoints for the implicit Theta, which was also tested on this problem but is not included here.

6.2.3. Viscous Burgers equation. The time-dependent viscous Burgers equation in one dimension is given by the partial differential equation

$$u_t - \nu \Delta u + u \nabla u = 0.$$

We follow here the work of [21], which was also performed in the framework of high-order spectral discretizations, albeit based on a Chebyshev grid and using discontinuous Galerkin; however the authors restrict themselves to very low-order polynomials, and their optimization algorithm does not exhibit the same acceleration as we achieve.

The idea is once again to choose an analytical solution and seek to converge to it in L_2 norm. The analytical solution is

$$(25) \quad u(x, t) = \frac{2\nu\pi \sin(\pi x) e^{-\nu t \pi^2}}{2 + e^{-\nu t \pi^2} \cos(\pi x)},$$

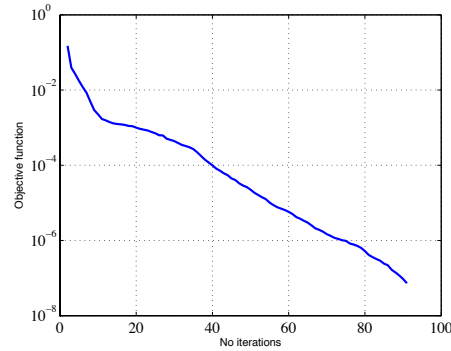
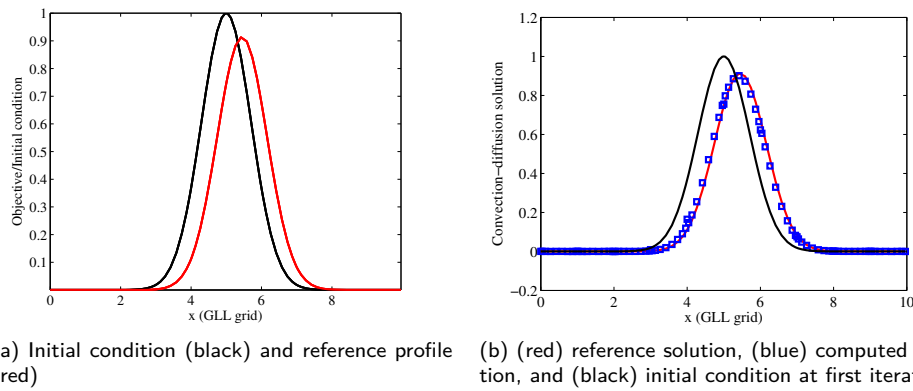


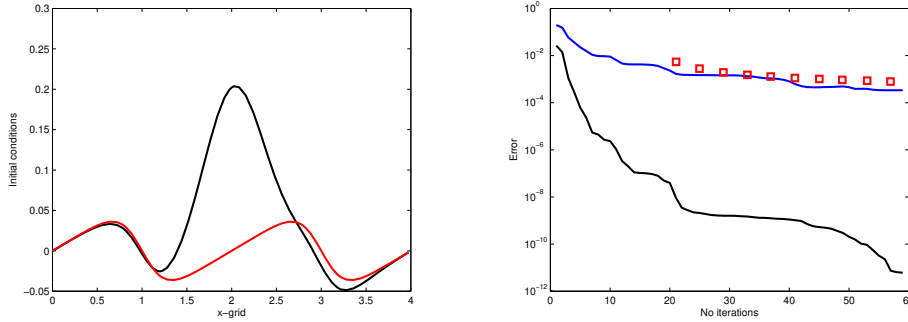
Figure 6: Objective function decay.

Figure 7: Optimal initial conditions for an advection-diffusion problem that fits a reference data at time horizon $T = 1$.

where the exact initial condition can be obtained for $t = 0$ and the time horizon set for $t = T$. We start from an initial condition that deviates from the analytical one by a Gaussian signal centered in the middle of the domain of interest $[-2, 2]$:

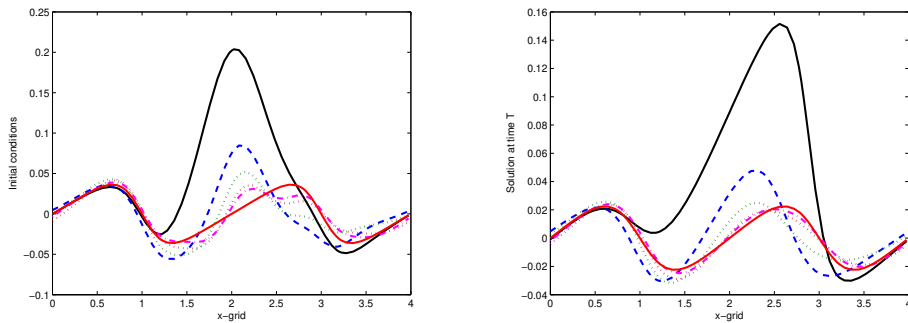
$$(26) \quad u(x, 0) = \frac{2\nu\pi \sin(\pi x)}{2 + \cos(\pi x)} + e^{-4(x-2)^2}.$$

In Figure 10 we study the h- and p-refinement convergence for Burgers equation



(a) Burgers equation, $T=4$ time horizon, optimal solution (red), initial condition at first iteration (black)
 (b) Objective function and initial condition error decay versus number of iterations; Data from [21] (red), error between computed initial condition and analytic initial condition (blue), objective function error (black).

Figure 8: Optimal initial conditions for Burgers equation with an analytic reference function up to time horizon $T=4$.



(a) Initial condition and evolution towards analytic initial condition.
 (b) Solution of Burgers equation and evolution toward the objective function.

Figure 9: Convergence of the solution for the first 4 iterations: (black) iteration 0, (blue) iteration 1, (green) iteration 2, (brown) iteration 3, (purple) iteration 4.

with a ν of 0.001. As expected, there is quadratic convergence with h-refinement and spectral with p-refinement. For this case we had to use the analytic initial conditions to get convergence to the discrete solution; using the previous perturbed Gaussian as initial conditions results in stagnation.

6.3. Two-dimensional viscous Burgers. The results and framework presented for the one-dimensional cases carry through to higher dimensions in a straightforward fashion. To exemplify this, we focus on the viscous Burgers equation, which is a prerequisite to Navier-Stokes and usually serves as a test case for incompressible flow problems. Since the viscous Burgers equation is nonlinear, the solution may quickly develop shocks. We

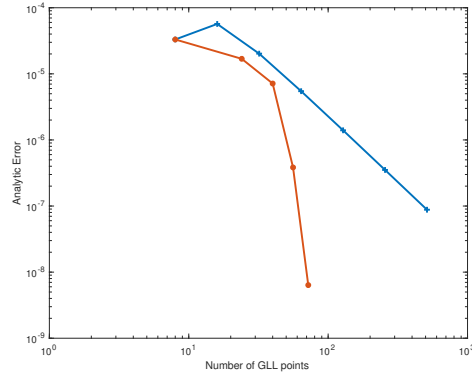


Figure 10: Convergence to the analytic optimal solution with h-refinement (blue) and p-refinement (red) for Burgers equation.

do not address such issues in the current work; instead we restrict ourselves to a smooth problem and choose an objective function that precedes a shock formation. We start with an initial condition, (see Figure 11a), given as

$$(27) \quad \begin{aligned} u(x, y, 0) &= e^{-\nu}(\cos(0.5\pi x) + \sin(0.5\pi y))/10 \\ v(x, y, 0) &= e^{-\nu}(\sin(0.5\pi x) + \cos(0.5\pi y))/10. \end{aligned}$$

The parameter is chosen such that it does not introduce severe damping while it does improve the stability region of the equation, $\nu = 5 \cdot 10^{-3}$. The objective is chosen to be the numerical solution obtained at the time horizon $T = 2$; see Figure 11b. The grid consists of 6 elements in both x and y directions, and each element is further discretized in $N = 8$ Gauss-Legendre-Lobatto points. Both the initial condition and objective function have the grid superposed on the velocity profile in Figure 11a.

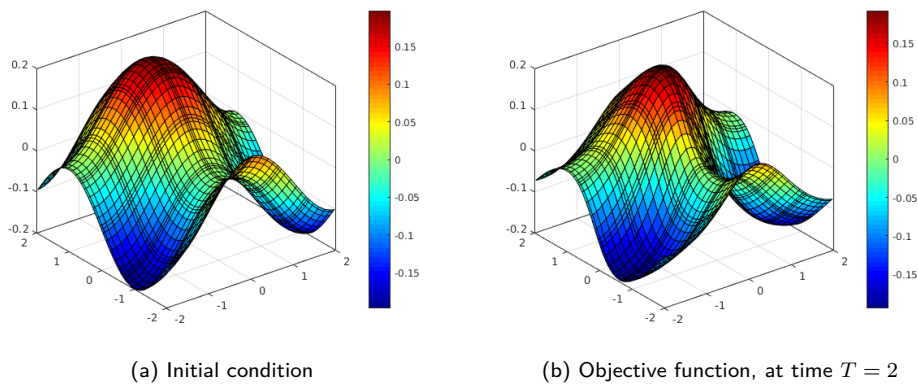
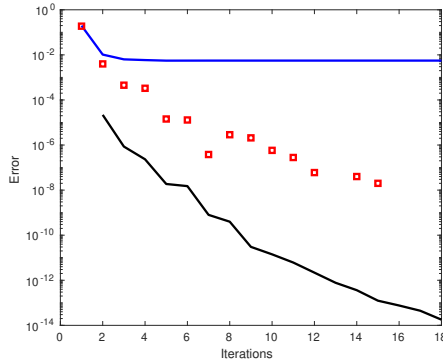


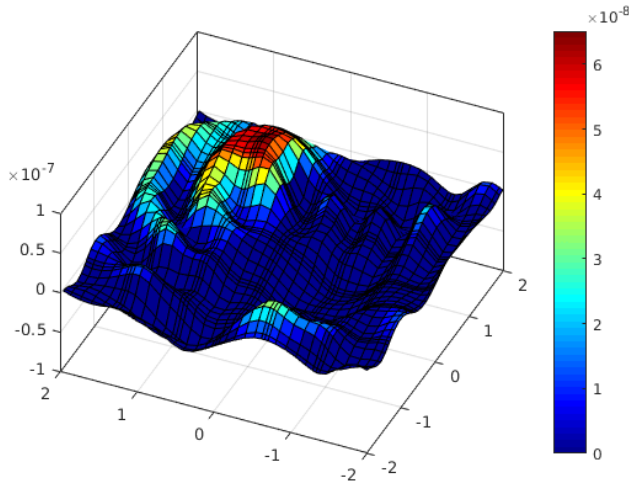
Figure 11: Component u of the solution to viscous Burgers equation.

The objective function is available as a data set and not as an analytical function. To analyze the relative error of the solution, we compute the L_2 error between each new

iterated initial condition and the original used for establishing an objective function; see Figure 12a. A comparison with the original analytical initial condition stagnates quickly around 10^{-3} , consistent with the one dimensional numerical experiment (Figure 8b). Comparing the analytical initial condition with the optimal one, we find that the decay is consistent with the decay in error in the objective function, as illustrated by red markers in Figure 12a.



(a) Error decay per iterations, in L_2 norm (black), comparison to original analytical initial condition (blue), difference in error for the initial condition (red markers).



(b) Gradient of the solution at iteration 15.

Figure 12: Convergence of the optimal initial conditions for viscous Burgers for a time horizon $T = 2$.

7. Conclusions. We have demonstrated how PETSc time integrators and adjoint capability and the gradient-based optimization capabilities of TAO can be used to systematically solve PDE-constrained optimization problems in both one and two dimensions discretized using the spectral element. This work focused on model problems for exposi-

tory reasons; the full power of PETSc solvers can be brought to bear for PDE-constrained optimization of more complex problems. Future work will tie error estimates from the spatial discretization with global error estimates in time [3] to produce global error estimates for the solution to the optimization problem.

Acknowledgments. We thank Hong Zhang, who implemented the adjoint capability in PETSc. This material is based upon work supported by the U.S. Department of Energy, Office of Science, Advanced Scientific Computing Research under Contract DE-AC02-06CH11357 and the Exascale Computing Project (Contract No. 17-SC-20-SC). This research was supported by the Exascale Computing Project (17-SC-20-SC), a collaborative effort of the U.S. Department of Energy Office of Science and the National Nuclear Security Administration.

REFERENCES

- [1] S. ABHYANKAR, J. BROWN, E. CONSTANTINESCU, D. GHOSH, B. SMITH, AND H. ZHANG, *PETSc/TS: A modern scalable DAE/ODE solver library*, Theoretical and Computational Fluid Dynamics Submitted, (2018).
- [2] S. BALAY, S. ABHYANKAR, M. F. ADAMS, J. BROWN, P. BRUNE, K. BUSCHELMAN, L. DALCIN, V. ELKHOUT, W. D. GROPP, D. KAUSHIK, M. G. KNEPLEY, D. A. MAY, L. C. MCINNES, R. T. MILLS, T. MUNSON, K. RUPP, P. SANAN, B. F. SMITH, S. ZAMPINI, H. ZHANG, AND H. ZHANG, *PETSc users manual*, Tech. Report ANL-95/11 - Revision 3.9, Argonne National Laboratory, 2018.
- [3] E. CONSTANTINESCU, *Generalizing global error estimation for ordinary differential equations by using coupled time-stepping methods*, Journal of Computational and Applied Mathematics, 332 (2018), pp. 140–158, <https://doi.org/https://doi.org/10.1016/j.cam.2017.05.012>, <http://www.sciencedirect.com/science/article/pii/S0377042717302480>.
- [4] M. O. DEVILLE, P. F. FISCHER, AND E. H. MUND, *High-Order Methods for Incompressible Fluid Flow*, Cambridge University Press, 2002, <http://dx.doi.org/10.1017/CBO9780511546792>. Cambridge Books Online.
- [5] I. DUNNING, J. HUCHETTE, AND M. LUBIN, *JuMP: a modeling language for mathematical optimization*, SIAM Review, 59 (2017), pp. 295–320.
- [6] R. FALGOUT, *hypr users manual*, Tech. Report Revision 2.11.2, Lawrence Livermore National Laboratory, 2017.
- [7] M. J. GANDER, F. KWOK, AND G. WANNER, *Constrained optimization: From Lagrangian mechanics to optimal control and PDE constraints*, in Optimization with PDE Constraints, Springer, 2014, pp. 151–202.
- [8] M. B. GILES AND N. A. PIERCE, *Adjoint equations in CFD: duality, boundary conditions and solution behaviour*, AIAA paper, 1850 (1997), p. 1997.
- [9] A. GRIEWANK AND A. WALTHER, *Algorithm 799: revolve: an implementation of checkpointing for the reverse or adjoint mode of computational differentiation*, ACM Transactions on Mathematical Software, 26 (2000), pp. 19–45.
- [10] M. D. GUNZBURGER, *Perspectives in flow control and optimization*, SIAM, 2002.
- [11] E. HABER AND L. HANSON, *Model problems in PDE-constrained optimization*, tech. report, TS-200X-00X-A, Emory University, 2007.
- [12] A. HINDMARSH, P. BROWN, K. GRANT, S. LEE, R. SERBAN, D. SHUMAKER, AND C. WOODWARD, *SUNDIALS: suite of nonlinear and differential/algebraic equation solvers*, ACM Transactions on Mathematical Software, 31 (2005), pp. 363–396.
- [13] O. R. ISIK, *Spin up problem and accelerating convergence to steady state*, Applied Mathematical Modelling, 37 (2013), pp. 3242–3253.
- [14] D. KOPRIVA, *Implementing spectral methods for partial differential equations: algorithms for scientists and engineers*, Springer Science & Business Media, 2009.
- [15] X. S. LI AND J. W. DEMMEL, *SuperLU_DIST: a scalable distributed-memory sparse direct solver for unsymmetric linear systems*, ACM Transactions on Mathematical Software, 29 (2003), pp. 110–140.
- [16] D. C. LIU AND J. NOCEDAL, *On the limited memory BFGS method for large scale optimization*, Mathematical Programming, 45 (1989), pp. 503–528.
- [17] C. MAVRIPLIS, *Proceedings of the Eighth GAMM-Conference on Numerical Methods in Fluid Mechanics*, Vieweg+Teubner Verlag, Wiesbaden, 1990, ch. A posteriori error estimators for adap-

- tive spectral element techniques, pp. 333–342.
- [18] J. J. MORÉ AND D. J. THUENTE, *Line search algorithms with guaranteed sufficient decrease*, ACM Transactions on Mathematical Software, 20 (1994), pp. 286–307.
 - [19] T. MUNSON, J. SARICH, S. WILD, S. BENSON, AND L. C. MCINNES, *Toolkit for Advanced Optimization (TAO) users manual*, Tech. Report ANL/MCS-TM-322 - Revision 3.9, Argonne National Laboratory, 2018.
 - [20] J. NOCEDAL AND S. J. WRIGHT, *Numerical Optimization*, Springer-Verlag, New York, 1999.
 - [21] K. OU AND A. JAMESON, *Unsteady adjoint method for the optimal control of advection and Burger's equations using high-order spectral difference method*, in 49th AIAA Aerospace Sciences Meeting including the New Horizons Forum and Aerospace Exposition, American Institute of Aeronautics and Astronautics, 2011.
 - [22] C. SAGLIETTI, P. SCHLATTER, A. MONOKROUSOS, AND D. S. HENNINGSON, *Adjoint optimization of natural convection problems: differentially heated cavity*, Theoretical and Computational Fluid Dynamics, (2016), pp. 1–17.
 - [23] A. SANDU, *On the properties of Runge-Kutta discrete adjoints*, in International Conference on Computational Science, Springer, 2006, pp. 550–557.
 - [24] M. SCHANEN, O. MARIN, H. ZHANG, AND M. ANITESCU, *Asynchronous two-level checkpointing scheme for large-scale adjoints in the spectral-element solver Nek5000*, Procedia Computer Science, 80 (2016), pp. 1147–1158.
 - [25] R. SERBAN AND A. C. HINDMARSH, *CVODES, the sensitivity-enabled ODE solver in SUNDIALS*, in Proceedings of the 5th International Conference on Multibody Systems, Nonlinear Dynamics and Control, Long Beach, CA, 2005.
 - [26] H. ZHANG AND A. SANDU, *FATODE: a library for forward, adjoint, and tangent linear integration of ODEs*, SIAM Journal on Scientific Computing, 36 (2014), pp. C504–C523.

Government License. The submitted manuscript has been created by UChicago Argonne, LLC, Operator of Argonne National Laboratory (“Argonne”). Argonne, a U.S. Department of Energy Office of Science laboratory, is operated under Contract No. DE-AC02-06CH11357. The U.S. Government retains for itself, and others acting on its behalf, a paid-up nonexclusive, irrevocable worldwide license in said article to reproduce, prepare derivative works, distribute copies to the public, and perform publicly and display publicly, by or on behalf of the Government. The Department of Energy will provide public access to these results of federally sponsored research in accordance with the DOE Public Access Plan. <http://energy.gov/downloads/doe-public-access-plan>.